Spanish Journal of Agricultural Research
17 (3), e0206, 13 pages (2019)
eISSN: 2171-9292
https://doi.org/10.5424/sjar/2019173-14357
Instituto Nacional de Investigación y Tecnología Agraria y Alimentaria (INIA)

RESEARCH ARTICLE

OPEN ACCESS

Harvest chronological planning using a method based on satellite-derived vegetation indices and artificial neural networks

Sepideh Taghizadeh (Taghizadeh, S)[1], Hossein Navid (Navid, H)[1], Reza Adiban (Adiban, R)[2] and Yasser Maghsodi (Maghsodi, Y)[3]

[1]University of Tabriz, Biosystems Engineering Dept., Tabriz 5166614776, Iran. [2]Agriculture Engineering Research Department, Ardabil Agricultural and Natural Resources Research and Education Center, AREEO, Ardabil (Moghan), Iran. [3]K.N. Toosi University of Technology, Photogrammetry and Remote Sensing Dept., Tehran, Iran.

Abstract

Aim of study: Wheat appropriate harvest date (WAHD) is an important factor in farm monitoring and harvest campaign schedule. Satellite remote sensing provides the possibility of continuous monitoring of large areas. In this study, we aimed to investigate the strength of vegetation indices (VIs) derived from Landsat-8 for generating the harvest schedule regional (HSR) map using Artificial Neural Network (ANN), a robust prediction tool in the agriculture sector.

Area of study: Qorveh plain, Iran.

Material and methods: During 2015 and 2016, a total of 100 plots was selected. WAHD was determined by sampling of plots and specifying wheat maximum yield for each plot. The strength of eight Landsat-8 derived spectral VIs (NDVI, SAVI, GreenNDVI, NDWI, EVI, EVI2, CVI and CI_{green}) was investigated during wheat growth stages using correlation coefficients between these VIs and observed WAHD. The derived VIs from the required images were used as inputs of ANNs and WAHD was considered as output. Several ANN models were designed by combining various VIs data.

Main results: The temporal stage in agreement with dough development stage had the highest correlation with WAHD. The optimum model for predicting WAHD was a Multi-Layer Perceptron model including one hidden layer with ten neurons in it when the inputs were NDVI, NDWI, and EVI2. To evaluate the difference between measured and predicted values of ANNs, MAE, RMSE, and R^2 were calculated. For the 3-10-1 topology, the value of R^2 was estimated 0.925. A HSR map was generated with RMSE of 0.86 days.

Research highlights: Integrated satellite-derived VIs and ANNs is a novel and remarkable methodology to predict WAHD, optimize harvest campaign scheduling and farm management.

Additional keywords: harvest date; Landsat-8 satellite; remote sensing; wheat.

Abbreviations used: ANN (artificial neural network); CI_{green} (green chlorophyll index); CVI (chlorophyll vegetation index); EVI (enhanced vegetation index); EVI2 (2 bands EVI); FLAASH (fast line-of-sight atmospheric analysis of spectral hypercubes); GDM (gradient descent with momentum); GreenNDVI (green normalized difference vegetation index); HSR (harvest schedule regional); MAE_p (mean absolute error for prediction); MLP (multi-layer perceptron); N (number of samples); NDVI (normalized difference vegetation index); NDWI (normalized difference water index); NIR (near-infrared); OLI (operational land imager); R (correlation coefficient); R_P^2 (coefficient of determination for prediction); $RMSE_p$ (root mean square error for prediction); SAVI (soil adjusted vegetation index); SWIR (short wave); STICS (simulateur mulltidiscplinaire pour les cultures standard); TANH (hyperbolic tangent); TIRS (thermal infrared sensor); VI (vegetation index); w (weight); WAHD (wheat appropriate harvest date); WOFOST (Worlds Food Study); $\bar{Y}_{est}$ (mean of estimated values of WAHD); $\bar{Y}_{mea}$ (mean of measured values of WAHD); Y_{mea} (measured WAHD); Y_{est} (estimated WAHD); α (momentum term); η (learning rate); o (output); δ (error).

Authors' contributions: Conceived and research design: ST, RA, and YM. Acquisition data and statistical analysis and writing: ST, RA. Critical revision of the manuscript for important intellectual content: ST, HN, RA. Coordinating and supervising the research work: HN, YM. All authors read and approved the final manuscript.

Citation: Taghizadeh, S; Navid, H; Adiban, R; Maghsodi, Y (2019). Harvest chronological planning using a method based on satellite-derived vegetation indices and artificial neural networks. Spanish Journal of Agricultural Research, Volume 17, Issue 3, e0206. https://doi.org/10.5424/sjar/2019173-14357

Received: 03 Dec 2018. **Accepted:** 14 Oct 2019.

Funding: University of Tabriz (Biosystems Engineering Dept.), Tabriz, Iran.

Competing interests: The authors have declared that no competing interests exist.

Correspondence should be addressed to Hossein Navid: navid@tabrizu.ac.ir

Introduction

Wheat (*Triticum aestivum* L.) is one of the most important cereals grown in the world. More humans consume wheat as their main food more than other cereal grains (Pimentel & Pimentel, 2007). So, wheat plays a very important role in the world's supply chain and food security. Therefore, maximum yield achievement at minimum expense is the main goal of wheat production. Awareness of crop growing dates, such as planting and harvesting dates, helps farm managers to reach the objectives and farm management. Harvest date is an important factor in field management. Planning the crop appropriate harvest date helps to schedule for harvest operation with less cost and maximize the profit (Abawi, 1993; Suwannachatkul *et al.*, 2014). In these studies, wheat appropriate harvest date (WAHD) is the date in which the wheat has reached maturity, and its moisture content is convenient for harvest by a combine harvester. In Iran, the appropriate moisture content is in the range of 12-14 percent (Mansouri-Rad, 2000). If wheat is harvested earlier than WAHD, there will be yield loss and its moisture content will be inappropriate for harvesting and storage (Burnett & Bakke, 1930; Philips & O'Callaghan, 1974; Sabir *et al.*, 2005). In contrast, harvesting after this date causes dry matter yield diminution and grain quality degradation. Moreover, yield loss due to weather conditions (such as temperature, rain, and wind), birds and insects damages to the matured product are disadvantages of delay in the harvest (BoIIand, 1984; Abawi, 1993; Farrer *et al.*, 2006; Sun *et al.*, 2007). In some areas of the world, the majority of farmers are smallholders, and the size of most agricultural farms is small. Consequently, it is not affordable for them to own their combine harvesters, leading to a shortage of harvesters in the harvest time (Bougari *et al.*, 2013). Lack of necessary machinery during harvest campaign could further delay the harvest date. Therefore, the wheat producers require prior planning for providing the combine harvester rental and labors which requires former notice of WAHD for each field. Field surveying operations are costly, time-consuming and infeasible in large areas to determine harvest date (Moran & Pearce, 1997; Pinter *et al.*, 2003). Some researchers (Porter & Gawith, 1999; McMaster& Wilhelm, 2003; Streck *et al.*, 2003; Evers *et al.*, 2010) have improved wheat phenological stages prediction models using photoperiod, water and vernalization to predict wheat maturity date. Other models such as STICS (Simulateur mulltidiscplinaire pour les Cultures Standard) and WOFOST (Worlds Food Study) have been developed by taking more factors into account such as temperature, nutrient and water stress for crop growth stage prediction (Boogaard *et al.*, 1998; Brisson *et al.*, 1998). Most of these models are based on meteorological parameters, making it difficult to discriminate within and between field differences in a dense configuration of the spatial grid (Meng *et al.*, 2015). Moreover, the main limitation of crop models is the challenges in preparing reliable input data. The uncertainty about the spatial repartition of soil properties and micro meteorological variables at farm scale limits these model output's assurance (Therond *et al.*, 2011).

Remote sensing provides appropriate and timely images of the agricultural farms. The higher revisit frequency capability is the merit of remote sensing (Atzberger, 2013) for collecting the farm information. In recent decades, satellite remote sensing has been applied for agricultural field management operations such as yield and biomass estimation (Panda *et al.*, 2010; Ren *et al.*, 2008; Xie *et al.*, 2009), phenological date prediction (Sakamoto *et al.*, 2010; De Bernardis *et al.*, 2016), and mapping of land use (Galford *et al.*, 2008; Atzberger & Rembold, 2013). Vegetation indices (VIs), which are computational combinations of different spectral bands of the electromagnetic spectrum, simplify the analysis and processing of big data obtained by satellites (Govaerts *et al.*, 1999; Viña *et al.*, 2011). The strong contrast of absorption and scattering of the red and near-infrared bands can be combined into different quantitative indices to explain the vegetation conditions. VIs are the semi-analytical measurements of plant vegetation activity which explain vegetation conditions during the growth stages. The benefit of VIs utilization is spectral reflectance data enhancement, by considering the variability of vegetation and minimizing of the atmospheric effect, sun-target-sensor geometry and soil (Moulin, 1999; Viña *et al.*, 2011).

The relationship between remote sensing indices and plant bio-physical variables is nonlinear (Haboudane *et al.*, 2004). Therefore, the usage of methods creating a non-linear relation between independent variables (VIs) and dependent variables could help predict better the plant bio-physical behavior changes. The artificial neural network (ANN) is the technique, widely used in the field of geo/bio-physical variable detections (Beale *et al.*, 2008). Application of ANN techniques using the VIs and also visible blue, green, red, near-Infrared (NIR) and short wave (SWIR) regions of the electromagnetic spectrum have led to successful results for crop monitoring, crop cover, crop growth, crop nitrogen, crop yield and biomass estimation (Chen & McNairn, 2006; Karimi *et al.*, 2006; Li *et al.*, 2007; Xie *et al.*, 2009; Prasad *et al.*, 2012). The aim of this study was to generate a harvest schedule regional (HSR) map for predicting WAHD by using two years (2015

& 2016) VIs data derived by operational land imager (OLI) sensor (Landsat-8) and ANN techniques.

Material and methods

Study site

The study was carried out in Qorveh plain in southeast of Kordestan province, West of Iran (35°15´N, 47°80´E), altitude 1900 m, with cold snowy winters and temperate summers (Fig. 1). The mean annual temperature of the site is 10.6 °C, and the average annual precipitation is 439 mm. The rainfed winter wheat is the major crop in this region, and it is sown in mid-October and harvested in mid-July of next year. The wheat-growing season is about 250 days.

Data acquisition

Field data

Field data for rainfed wheat yield measurement was collected during the wheat maturing stage of 2015 and 2016 years (from June 19 to July 11). Fifty sampling plots were selected from fifty wheat farms, in each year. They were flat and homogenous with areas bigger than 175×175 m^2. The size of plots chosen was 60×60 m^2 and plots were located at the center of wheat farms. A GPS receiver (Garmin GPSMAP 62s, Taiwan, with a spatial accuracy 3 m) was used for recording the geo-coordinates of each plot. The plant density in each plot was obtained in early June using a 1 m × 1 m quadrate. The plant density measurements were done by ten times random throwing of the quadrate through the zigzag sweep path and counting the number of plants in each throw and averaging of plant numbers of the quadrates. According to the field observations, plant densities often were constant on each farm.

The yield sampling was carried out by five random throws of the quadrate and choosing three plants in each throw. The plants were randomly chosen in the quadrate. At each sampling, fifteen plants were sampled for each plot, in total. By measuring the average grain weight of sampled plants in each plot and knowing plant density, the yield amount was acquired for each plot. The grains were used to measure the yield of fully matured plants. The sampling operation was conducted at a frequency of 2 days, from June 19 to July 11. Generally, eleven yield sampling observations were carried out for each plot in each year. The interpolation between yield observations was done by fitting a spline curve. The WAHD was considered the day of wheat highest yield.

Satellite image acquisition and pre-processing

Landsat-8 is the latest in a series of Landsat satellites, and it was launched on February 11, 2013 (http://science.nasa.gov/missions/ldcm). The operational land imager (OLI) and the thermal infrared sensor (TIRS) are two sensors which are carried by the Landsat-8 (Roy *et al.*, 2014). We used OLI sensor data in this study. The appropriate spatial resolution of OLI in comparison with the common size of agricultural farms is its advantage for using in agricultural studies. OLI consist of nine spectral bands. The spatial resolution for bands 1 to 7 (coastal, blue, green, red, NIR, SWIR1, SWIR2) and band 9 (cirrus), is 30 m and for panchromatic band (band 8) is 15 m. A series of OLI images of the

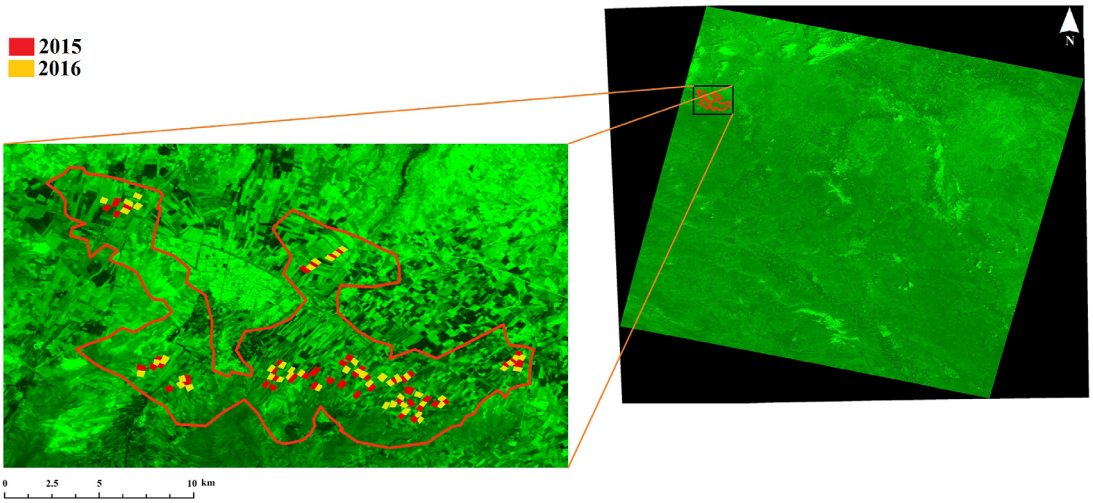

Figure 1. Study site and sampling farm locations. Background: Landsat-8 OLI at 17 May 2016 (Row: 36, Path: 166).

study area (path: 166, 167 & row: 35, 36) was acquired after wheat dormancy stage with no cloud or less than 10% amount of cloud in each year. The images were acquired in 2015 on April 4, April 20, April 29, May 6, May 31, June 7, June 16 and June 23 which there were coincided with tillering, stem extension (20th & 29th of April), booting, heading, dough development, physiological maturity and harvest ripe stages of wheat, respectively. Also, in 2016 the images on April 6, April 22, May 1, May 8, May 17, June 9, June 18 and June 25 were acquired which there were coincided with tillering, stem extension (22th of April & 1st of May), booting, heading, dough development, physiological maturity and harvest ripe stages of wheat, respectively.

The pre-processing of images was performed in ENVI 5.1 software. Since the OLI images had been corrected geometrically, we just did the second geo-referencing operation to ensure the correct location of terrain. The ground control points derived from 1:25000 topographic maps were applied for geometric correction. The geo-correction error less than 0.5 pixel (15 m) was attained. The nearest neighbor method and linear polynomial geometric model were used. Atmospheric corrections were performed using MODTRAN 4 model in FLAASH (Fast Line-of-sight Atmospheric Analysis of Spectral Hypercubes) module in the ENVI 5.1. The parameters used in the FLAASH were adjusted based on scene center location, sensor type, sensor altitude, ground elevation, pixel size, information about sensor flight date and weather conditions on the image acquisition date. The output of the FLAASH package was the surface reflectance of OLI images.

Extraction of vegetation indices

There are some studies which have suggested double or multi-band spectral indices to estimate bio-physical changes of crops (Garroutte *et al.*, 2016; Li *et al.*, 2016). This study included eight widely used VIs to investigate the strength of VIs during wheat growing stages. These indices included: NDVI (normalized difference vegetation index), SAVI (soil adjusted vegetation index), EVI (enhanced vegetation index), EVI2 (2 bands enhanced vegetation index), NDWI (normalized difference water index), GreenNDVI (green normalized difference vegetation index), CVI (chlorophyll vegetation index) and CI_{green} (green chlorophyll index). The VIs mentioned above can be classified in three groups based on their sensitivity to green biomass (NDVI, SAVI, EVI, EVI2), the liquid water content of vegetation (NDWI) and leaf chlorophyll (CVI, GreenNDVI, and CI_{green}). Table 1 represents the formula of these indices.

Determining the best temporal stage for WAHD prediction

In each year, to determine the best temporal and phenological stage for predicting WAHD, correlation coefficients (R) between VIs and WAHD were calculated for different images acquired during the wheat growth phases. The date with the highest *R* values was recognized as the best temporal stage for WAHD prediction.

The artificial neural network model

The ANNs are flexible mathematical models that accomplish a computational simulation based on the behavior of human brain neurons. The ANN is a non-linear machine learning algorithm with a high potential for modeling and prediction (Foody, 2004). It is composed of artificial neuron groups which are interconnected with weighted links and could create a strong relation between inputs and outputs using a learning approach (Omer *et al.*, 2016). The network architecture is the first step for developing an ANN model that is determined by artificial neurons and layers.

Table 1. Formula for several spectral vegetation indices.

Vegetation index	Formula	Reference
NDVI	$NDVI = (\rho_{NIR} - \rho_{Red})/(\rho_{NIR} + \rho_{Red})$	Rouse *et al.*, 1974
SAVI	$SAVI = (\rho_{NIR} - \rho_{Red})(1 + L)/(\rho_{NIR} + \rho_{Red} + L)$	Huete, 1988
EVI	$EVI = 2.5\ (\rho_{NIR} - \rho_{Red})/(\rho_{NIR} + 6\rho_{Red} - 7.5\rho_{Blue} + 1)$	Huete *et al*., 1997
EVI2	$EVI2 = 2.5\ (\rho_{NIR} - \rho_{Red})/(\rho_{NIR} + 2.4\rho_{Red} + 1)$	Jiang *et al*., 2008
NDWI	$NDWI = (\rho_{NIR} - \rho_{SWIR})/(\rho_{NIR} + \rho_{SWIR})$	Gao, 1996
CVI	$CVI = (\rho_{NIR}/\rho_{Green}) * (\rho_{Red}/\rho_{Green})$	Vincini *et al*., 2007
GreenNDVI	$GreenNDVI = (\rho_{NIR} - \rho_{Green})/(\rho_{NIR} + \rho_{Green})$	Gitelson & Merzlyak, 1998
CI_{green}	$CIGreen = (\rho_{NIR}/\rho_{Green}) - 1$	Gitelson *et al.*, 2003

ρ_{Blue}, ρ_{Green}, ρ_{Red}, ρ_{NIR} and ρ_{SWIR} are spectral reflectance of red, green, blue, near infrared and short wave infrared bands which are in accordance with bands 2, 3, 4, 5 and 6 for OLI sensor, respectively.

A usual ANN consists of an input layer, an output layer, and several hidden layers. Also, each layer contains some neurons and activation functions. In this study, we used a Multi-layer perceptron (MLP) network which is extensively used type of ANNs in the community of remote sensing. The gradient descent with momentum (GDM) algorithm was used to train the network. For this algorithm, the weights are updated during the nth training iteration as follows (Omid *et al.*, 2009):

$$w_{ij}^{(n)} = w_{ij}^{(n-1)} + \Delta w_{ij}^{(n)} \quad (1)$$

Additionally, the set of weights are given by:

$$\Delta w_{ij}^{(n)} = \eta \delta_j^{(n)} o_i^{(n)} + \alpha \Delta w_{ij}^{(n-1)} \quad (2)$$

where $w_{ij}^{(n)}$ is the weight between the jth neuron of the upper layer and the ith neuron of the lower layer, δ_j is the error of j^{th} neuron, o_i is the output value of the ith neuron of the previous layer, η is the learning rate and α is the momentum term. $\Delta w_{ij}^{(n)}$, is the gradient vector affiliated with the weights.

ANNs structure

To consider the efficacy of inputs (Green biomass sensitive, chlorophyll sensitive and water content sensitive VIs) on WAHD prediction, eight MLP type models were designed. Fig. 2 shows a typical scheme of an MLP model which comprises the input layer, the hidden layer, and the output layer. Different models were designed using various combination of VIs as the neurons in the input layer (ANN-1 to ANN-8). The input variables for ANN-1 to ANN-3 were green biomass sensitive VIs, chlorophyll sensitive VIs and water content sensitive VIs, respectively. The input variables for ANN-4 were EVI2 (green biomass sensitive), NDWI (water content sensitive) and GreenNDVI (chlorophyll sensitive) that each of them had the highest correlation with the observed WAHD in their groups. The input variables for ANN-5 was a combination of the NDVI and EVI2 (green biomass sensitive) and NDWI (water content sensitive). ANN-6 was a combination of green biomass sensitive VIs (NDVI, SAVI, EVI2) and chlorophyll sensitive VI (GreenNDVI). The input variables for ANN-7 were the combination of chlorophyll sensitive and water content sensitive VIs. The input variables for ANN-8 were the combination of green biomass sensitive and water content sensitive VIs (Table 2).

For determining the optimum number of hidden layer neurons, the minimum value of RMSE was considered. In this study, the used activation function was hyperbolic tangent (TANH) for hidden and output layers. Also, the values of α=0.7 and η=0.1 were used.

The data set on 100 VIs for predicting WAHD was split into three parts: 70% of VIs for training, 15% for cross-validation and 15% for testing data. After sufficient training, the weights of the network were adapted and applied for validation to determine the model overall performance.

ANN model performance and validation

The performance of eight ANN constructed model using a different number of VIs was evaluated by statistical parameters including coefficient of determination for prediction (test data) (R_P^2), mean absolute error for prediction (MAE_p), and the root mean square error for

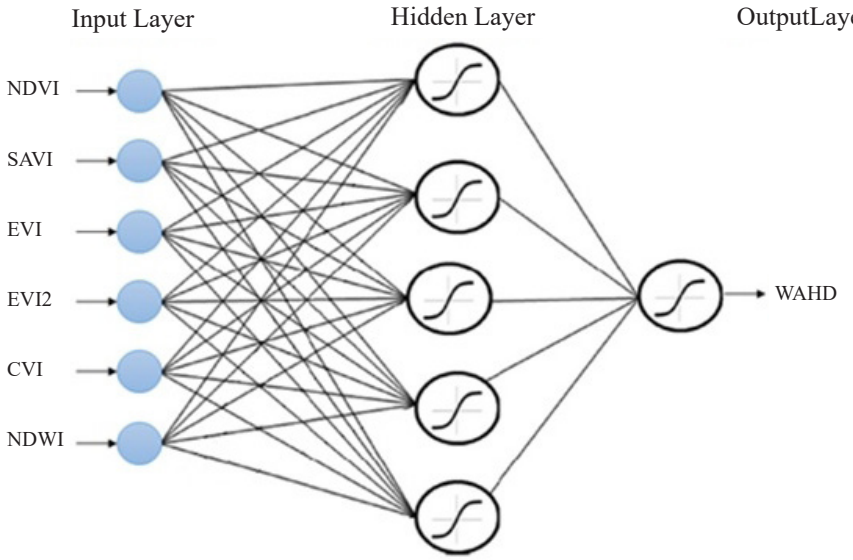

Figure 2. Scheme of the multi-layer perceptron (MLP) model structure used for wheat appropriate harvest date (WAHD).

Table 2. Combination of various VIs data as inputs of estimated ANN models.

Prediction model	NDVI	SAVI	EVI	EVI2	GreenNDVI	CVI	CI_{green}	NDWI
ANN-1	■	■	■	■				
ANN-2					■	■	■	
ANN-3								■
ANN-4				■	■			■
ANN-5	■			■				■
ANN-6	■	■		■	■			■
ANN-7					■	■	■	■
ANN-8	■	■	■	■				■

prediction ($RMSE_p$). The values of R_P^2, MAE_p, and $RMSE_p$ were calculated using equations 3, 4 and 5, respectively.

$$R_P^2 = \frac{\left(\sum_{i=1}^{N}\left(Y_{est,i} - \bar{Y}_{est,i}\right)\left(Y_{mea,i} - \bar{Y}_{mea,i}\right)\right)^2}{\sum_{i=1}^{N}\left(Y_{est,i} - \bar{Y}_{est,i}\right)^2 \sum_{i=1}^{M}\left(Y_{mea,i} - \bar{Y}_{mea,i}\right)^2} \quad (3)$$

$$MAE_P = \frac{\sum_{i=1}^{N}\left|Y_{est,i} - Y_{mea,i}\right|}{N} \quad (4)$$

$$RMSE_P = \sqrt{\frac{\sum_{i=1}^{N}\left(Y_{est,i} - Y_{mea,i}\right)^2}{N}} \quad (5)$$

where $Y_{mea,i}$ is the measured WAHD, $Y_{est,i}$ is the estimated WAHD, $\bar{Y}_{mea,i}$ is the mean of measured values of WAHD, $\bar{Y}_{est,i}$ is the mean of estimated values of WAHD, and N is the number of samples. The higher values for R_P^2 and lower values of MAE_p and RMSEp represent further precision and accuracy of the model. All calculations for ANN models were implemented using custom-written scripts of MATLAB R2015a software.

Harvest schedule regional (HSR) map

The predicted data of the best MLP model (in terms of precision and accuracy) was used for generating the HSR map using ArcGIS 10 software. Furthermore, the WAHD map was provided using the data of the test set. Moreover, both of the generated maps were compared with maps of measured data.

Results

The best temporal stage for WAHD prediction

Table 3 and Table 4 show the variation of *R*-values between VIs and observed WAHD in 2015 and 2016, respectively. The *R*-values were calculated to specify which temporal stage and VIs are appropriate for WAHD prediction. Also, for better comprehend the results in Tables 3 and 4, the temporal variations of *R*-values were presented in Fig. 3. Most of *R*-values had an ascendant trend before Jun 7, 2015 (Fig. 3a), and Jun 9, 2016 (Fig. 3b). However, a decline was observed in *R*-values after these dates. Based on the results the days of early of June were the best temporal phase for WAHD prediction which was coincided with dough development stage of wheat.

In 2015, the maximum *R*-values for NDVI, SAVI, EVI, EVI2, GreenNDVI, CI_{green}, and NDWI were 0.729, 0.698, 0.744, 0.758, 0.594, 0.558 and 0.753 respectively

Table 3. The *R* values between WAHD and various VIs at different dates in 2015. The maximum *R* values are in bold type.

Vis 2015	Apr 4	Apr 20	Apr 29	May 6	May 31	Jun 7	Jun 16	Jun 23
NDVI	0.341	0.376	0.377	0.511	0.625	**0.729**	0.564	0.412
SAVI	0.298	0.401	0.392	0.456	0.607	**0.698**	0.618	0.441
EVI	0.376	0.369	0.395	0.524	0.664	**0.744**	0.628	0.514
EVI2	0.345	0.384	0.389	0.557	0.668	**0.758**	0.632	0.513
GreenNDVI	0.179	0.241	0.298	0.439	0.459	**0.594**	0.466	0.404
CVI	0.197	0.310	0.309	0.329	0.435	0.423	**0.563**	0.437
CI_{green}	0.067	0.183	0.138	0.236	0.401	**0.558**	0.444	0.351
NDWI	0.175	0.208	0.257	0.379	0.627	**0.753**	0.608	0.356

Table 4. The *R* values between WAHD and various VIs at different dates in 2016. The maximum *R* values are in bold type.

VIs 2016	Apr 6	Apr 22	May 1	May 8	May 17	Jun 9	Jun 18	Jun 25
NDVI	0.334	0.412	0.468	0.514	0.592	**0.698**	0.501	0.357
SAVI	0.330	0.361	0.410	0.478	0.517	**0.686**	0.551	0.473
EVI	0.409	0.326	0.319	0.480	0.597	**0.709**	0.506	0.467
EVI2	0.360	0.371	0.410	0.532	0.605	**0.763**	0.607	0.522
GreenNDVI	0.216	0.221	0.249	0.419	0.425	0.560	**0.582**	0.455
CVI	0.165	0.257	0.314	0.380	0.444	0.530	**0.554**	0.541
CI_{green}	0.114	0.169	0.278	0.312	0.335	0.482	**0.541**	0.480
NDWI	0.203	0.286	0.301	0.418	0.601	**0.747**	0.568	0.455

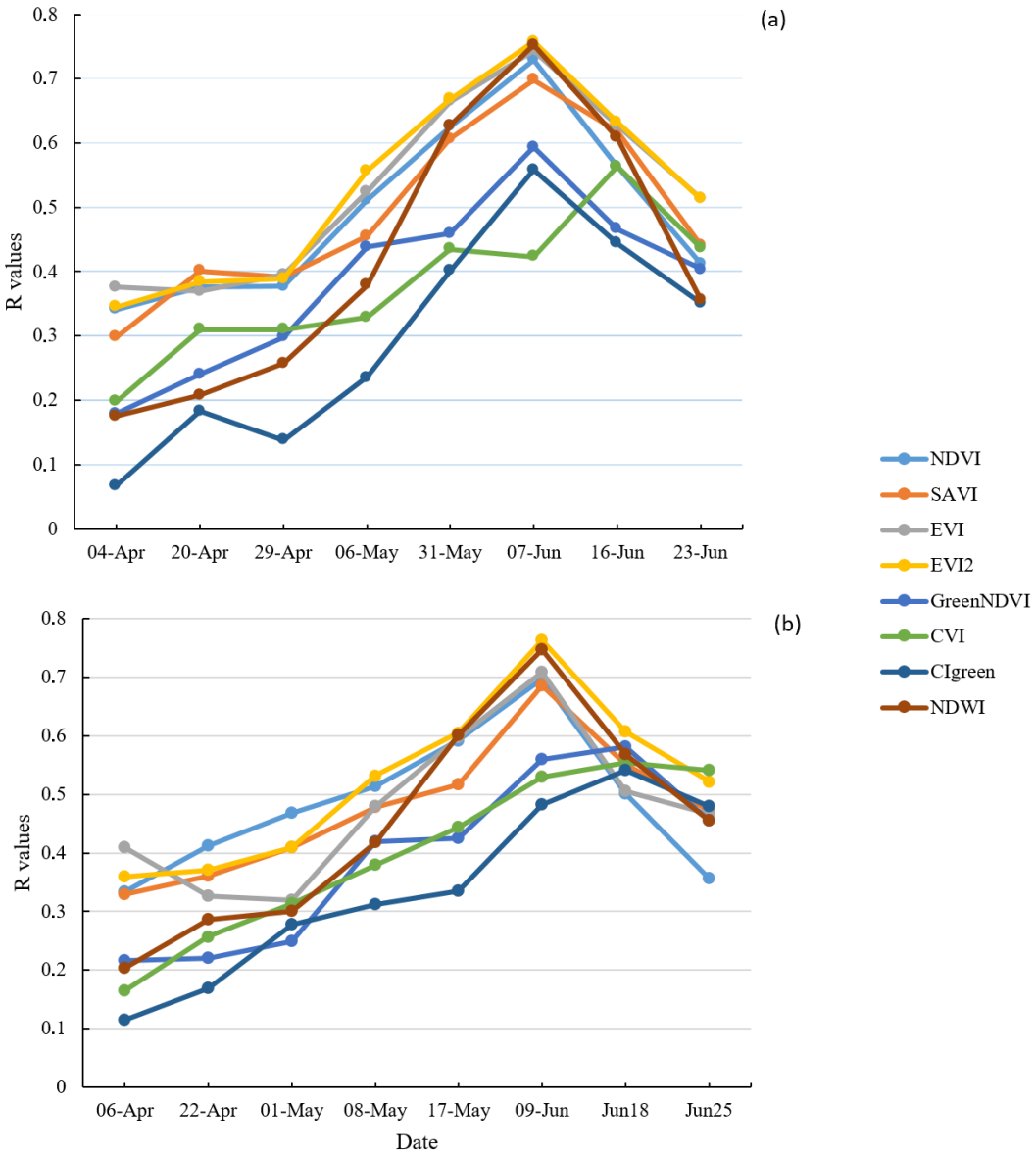

Figure 3. Temporal variations of *R* values between WAHD and VIs (a) in 2015 and (b) in 2016.

that were obtained on Jun 7, but the *R*-value of CVI (0.563) was maximum on Jun 16 (Table 3).

As shown in Table 4, the maximum *R*-values were achieved on Jun 9 for NDVI (0.698), SAVI (0.686), EVI (0.709), EVI2 (0.763), and NDWI (0.747) in 2016. Additionally, the maximum of R-values for GreenNDVI, CVI, and CI_{green} were 0.582, 0.554 and 0.541 on Jun 18. Considering the *R*-value as an indicator to assess the ability of VIs to estimate WAHD at wheat different growth stages, the June 7, 2015, and June 9, 2016, was selected for prediction.

Evaluation of ANN models

The results of designed models and the R_P^2, MAE_P, and $RMSE_P$ values for these models are summarized in Table 5. For these models, R_P^2, MAE_P and $RMSE_P$ values ranged from 0.611 to 0.925, 0.70 to 1.51, and 0.87 to 2.00, respectively. From the designed and trained networks, the ANN-5 presented better results than other networks. Therefore, the ANN-5 was selected as the best estimation model for WAHD (eq. 6):

$$WAHD_{ANN-5} = \sum_{j=1}^{10} w_j^{(O)} f\left(\sum_{i=1}^{3} w_{ji}^{(h)}.f(net_i) + w_{jO}^{(h)}\right) + w_O^{(O)} \quad (6)$$

where $WAHD_{ANN-5}$ is the predicted value of the *WAHD* using the ANN-5, and $f(net_i)$ is tanh (net_i). Hence, the (1- 10-3) - MLP network, consists of three VIs as input variables (EVI2, NDWI, NDVI), ten neurons in the hidden layer and a single output variable (WAHD) was selected as the optimum network. The values of R_P^2, MAE_P, and $RMSE_P$ for this topology were obtained 0.925 (Fig. 4b), 0.70 and 0.87, respectively. Fig. 4a shows the comparison between predicted WAHD values (test data) with the measured data. It could be observed that the trends were similar and superimposed over the others in some parts. The second model that had good performance for WAHD estimation was ANN-8 (R_P^2 =0.882; MAE_P=1.05; $RMSE_P$=1.11). Three VIs (NDVI, EVI2, and NDWI) were common parameters for both models ANN-5 and ANN-8. In other words, NDVI, EVI2, and NDWI can predict WAHD better than other indices.

ANN-2 (R_P^2=0.706; MAE_P=1.51; $RMSE_P$=2.00) which included GreenNDVI, CVI, and CI_{green} had low accuracy for WAHD modeling. Therefore, it can be concluded that GreenNDVI, CVI, and CI_{green} are not good indicators for WAHD prediction. In addition, ANN-3 model with individual input (NDWI) did not have high accuracy estimation for WAHD (R_P^2=0.611; MAE_P=1.41; $RMSE_P$=1.86). But, it can be seen in ANN-7 model that adding NDWI to GreenNDVI, CVI, CI_{green} VIs (ANN-2) led to better estimations for WAHD prediction (R_P^2=0.759; MAE_P=1.22; $RMSE_P$=1.49). Besides, by adding the NDWI to vegetation indices of ANN-1, the accuracy of model improved ANN-8 (Table 5). In total, it is concluded that NDWI composition with other indicators could improve the forecast of WAHD.

HSR map

The HSR map using all data is shown in Fig. 5b, where ANN-5 model has been used for estimation as respects it had the best prediction accuracy (as explained in detail earlier). Also, the comparison between measured and estimated HSR maps is presented in Fig. 5, where the ANN-5 shows to have made good estimations of WAHD. Also, the trend of harvesting dates for different farms is the same in the two maps (Fig. 5).

As shown in estimated and measured maps (Fig. 5), the WAHD of northern regions is after the southern regions. Therefore, the harvest operation should start from the farms in southeast regions in the maps and completed in northwest farms. The differences in sowing dates, topographic variations, and the angle of sunlight, temperature, precipitation and soil moisture

Table 5. The value of R^2 and RMSE for different simulations between measured and estimated ANN-models. ANN-5 (bolded) was selected as the best estimation model.

Prediction model	Best structure of MLP	R_P^2	MAE_P	$RMSE_P$
ANN-1 (NDVI, SAVI, EVI, EVI2)	1-10-4	0.857	1.06	1.12
ANN-2 (CVI, GreenNDVI, CI_{green})	1-13-3	0.706	1.51	2.00
ANN-3 (NDWI)	1-8-1	0.611	1.48	1.86
ANN-4 (EVI2, NDWI, GreenNDVI)	1-12-3	0.844	0.99	1.08
ANN-5 (EVI2, NDWI, NDVI)	**1-10-3**	**0.925**	**0.70**	**0.87**
ANN-6 (NDVI, EVI2, SAVI, GreenNDVI, NDWI)	1-16-5	0.843	1.13	1.38
ANN-7 (GreenNDVI, CVI, CI_{green}, NDWI)	1-14-4	0.759	1.22	1.49
ANN-8 (NDVI, SAVI, EVI, EVI2, NDWI)	1-13-5	0.882	1.05	1.11

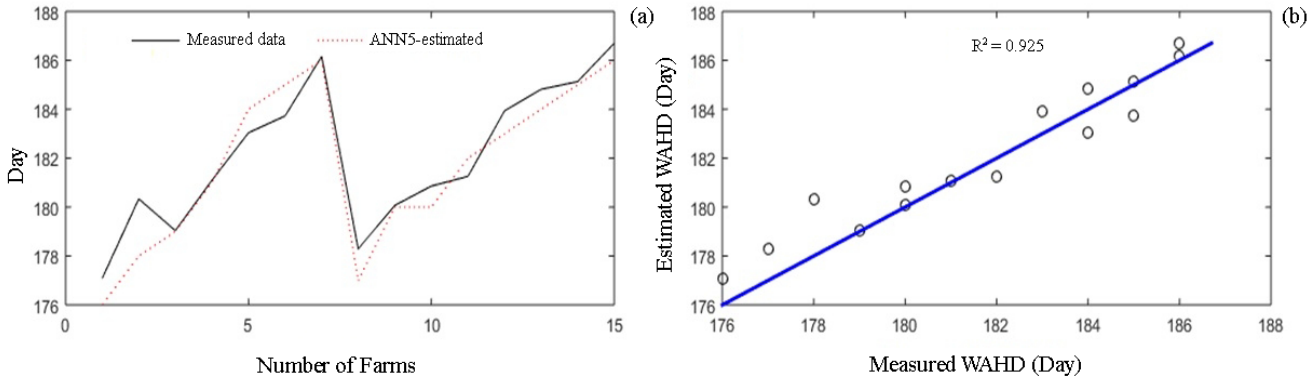

Figure 4. (a) Estimated (ANN-5) and measured WAHD on testing data. (b) Measured *vs*. estimated WAHD values (ANN5).

amount are the reasons of WAHD variation among these farms.

The estimated (using test data of ANN-5) and measured WAHD maps are shown in Fig. 6a and 6b, respectively. As seen in Fig. 6, the ANN-5 could provide very good predictions of WAHD. However, there were few differences between measured and estimated WAHD, and one disagreement was labeled with a black circle in Fig. 6. Therefore, it can be concluded that the MLP model with 1-10-3 topology had very good performance for harvest date predictions.

Discussion

In this study, we present a method for predicting WAHD, based on Landsat-8 derived VIs and ANNs to optimize harvest campaign scheduling and farm management. The utilized approach is based on the spectral variation of wheat canopy during phenological stages. The VIs, using the combination of different spectral bands, could explain the vegetation conditions during wheat growth stages. The VIs used in this study were classified in three groups based on their sensitivity to green biomass (NDVI, SAVI, EVI, EVI2), the liquid water content of vegetation (NDWI) and leaf chlorophyll (CVI, GreenNDVI, and CI_{green}).

In the present study, application of ANNs, as non-linear modeling techniques, had excellent performance for estimating WAHD. The performance and accuracy of MLP models to WAHD estimation was due to the key features of these type models: (i) the intrinsic abilities of ANNs, such as learning, cross-validating and flexible processing; (ii) generating non-linear patterns between inputs and outputs which lead to accurate estimations of complex and dynamic data; and (iii) the VIs included intensive data which correlate non-linearly with spatial based WAHD. Therefore, considering the nature of VIs data, the ANN modeling techniques are a very good substitute for linear statistical methods. As reported

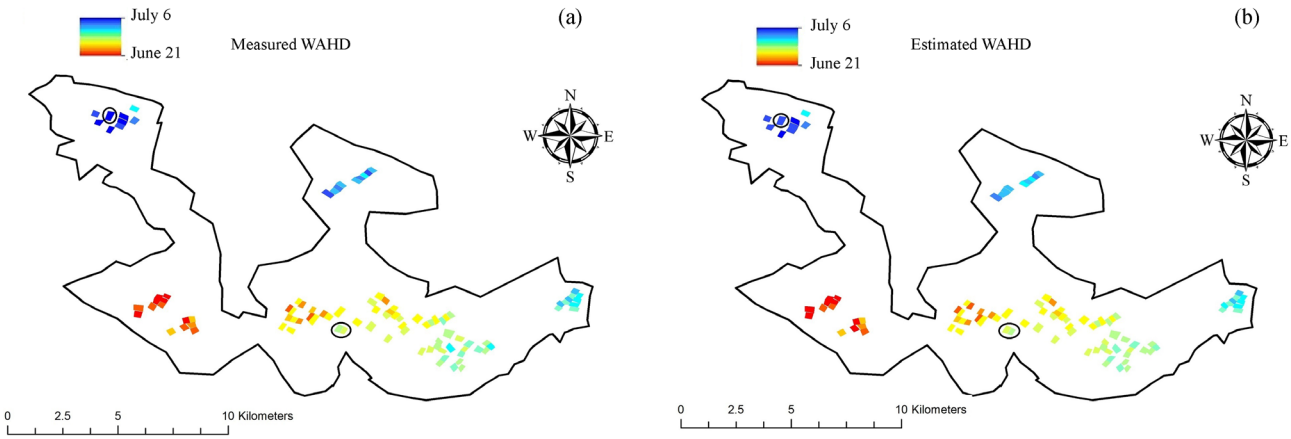

Figure 5. Comparison between measured (a) and estimated (using ANN-5) (b) HSR maps for All data.

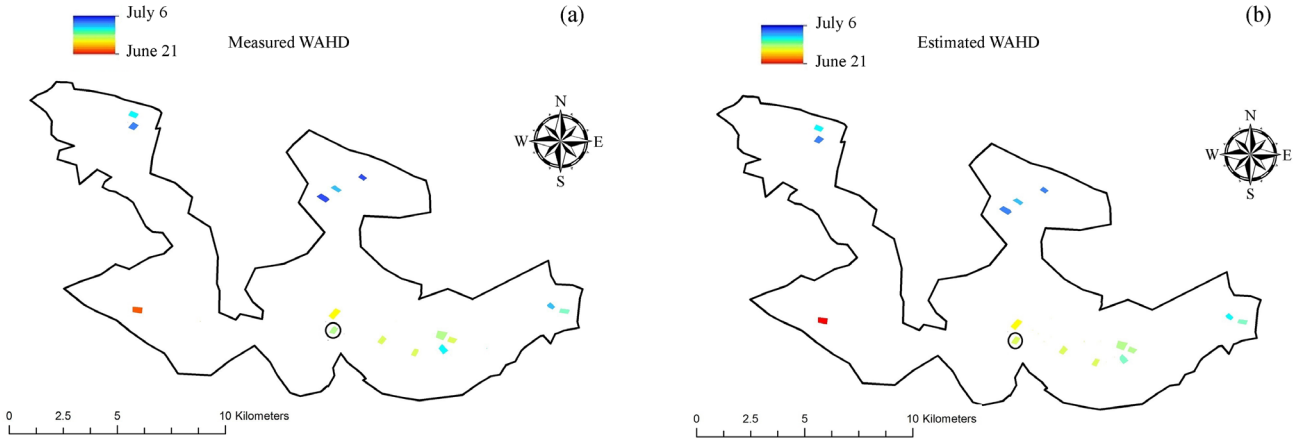

Figure 6. Comparison between measured (a) and estimated (using ANN-5) (b) WAHD maps for Test data.

by Xie *et al.* (2009), the ANN models could provide an accurate estimation (R^2=0.817 and RMSE=0.4236) for predicting above ground grassland biomass based on Landsat ETM+. Also, other researches which have been done using ANN techniques and VIs, suggest that utilizing of ANNs in remote sensing applications, has been very successful in the agriculture sector (Li *et al.*, 2007; Fortin *et al.*, 2010; Pantazi *et al.*, 2016).

The ANN-5 had the best estimation of WAHD. The input variables of this model were EVI2, NDWI, and NDVI. EVI2 could be recognized as the best index for WAHD prediction because of its high *R* value with WAHD. EVI2 consists of NIR and red bands; strong contrast of leaf scattering in the NIR wavelength and chlorophyll absorption in the red wavelength, makes EVI2 very robust to explain the vegetation conditions. EVI2 not only has an improved sensitivity over high biomass, in comparison with the SAVI, but also minimizes soil influences (Jin *et al.*, 2016). EVI2 can capture subtle changes in vegetation structure and condition, especially to discriminate between leaf area index surface and greenness for vegetation with various soil background reflectances (Rocha & Shaver, 2009). Therefore, EVI2 is a suitable indicator for WAHD prediction. Results achieved by Bolton & Friedl (2013) as well as by Wang *et al.* (2015), proved that EVI2 has a high ability to predict maize yield and estimate rice phenology, respectively. NDWI is sensitive to the total amounts of the liquid water content of vegetation canopies (Gao, 1996). The water content of wheat canopy varies during wheat growth stages, and NDWI could present these water content variations. As reported by Liu *et al.* (2006) and Bao *et al.* (2008), NDWI had a good correlation with wheat biophysical parameters and yield. Although in the present study NDWI did not have a good ability to WAHD estimation alone (ANN-3 model; R_P^2=0.611; MAE_p=1.41; $RMSE_p$=1.86), adding NDWI to other indices improved the estimation power of models (ANN-2 *vs*. ANN-7 and ANN1 *vs*. ANN8). NDVI is the most practical indicator which is widely used in vegetation monitoring. According to Suwannachatkul *et al.* (2014), the use of NDVI to estimate rice harvest date resulted in acceptable accuracy (about eight days). NDVI was the only indicator used for predicting. The results of the current study showed that the combination of VIs for WAHD prediction improved the estimation accuracy (about one day). This was also confirmed in the present study, where green biomass sensitive VIs (NDVI, SAVI, EVI, EVI2) could estimate WAHD better than chlorophyll sensitive VIs (CVI, GreenNDVI, CI green) by comparing models ANN-1 and ANN-2. Moreover, ANN-6 and ANN-7 represent this issue. Therefore, it is suggested that biomass-sensitive VIs be used in the harvesting date prediction researches.

The methodology applied in this paper is straightway and just needs satellite imagery bands to predict WAHD. The substantial advantage of the used method is its relative simplicity which makes it suitable for regional scale applications. The present method can be extended to other regions of the world. Also, other satellite sensors can be applied with this method. Moreover, the current model (ANN-5) may be helpful to regions with similar climate, where the sowing and harvesting dates are similar to the study region. The main limitation of this method is the accessibility of valid satellite imagery. The cloudy weather disrupts access to satellite images. A solution to this problem is the simultaneous use of several satellite images (Shang *et al.*, 2014; Wang *et al.*, 2015).

The current study presents a preliminary investigation of WAHD using satellite imagery. This method can be applied to other crops considering the crop conditions. Also, the combination of satellite remote sensing

models, crop models, and meteorological statistical models will improve predictions.

References

Abawi GY, 1993. A simulation model of wheat harvesting and drying in northern Australia. J Agric Eng Res 54: 141-158. https://doi.org/10.1006/jaer.1993.1009

Atzberger C, 2013. Advances in remote sensing of agriculture: Context description, existing operational monitoring systems and major information needs. Remote Sens 5: 949-981. https://doi.org/10.3390/rs5020949

Atzberger C, Rembold F, 2013. Mapping the spatial distribution of winter crops at sub-pixel level using AVHRR NDVI time series and neural nets. Remote Sens 5: 1335-1354. https://doi.org/10.3390/rs5031335

Bao Y, Liu L, Wang J, 2008. Estimating biophysical and biochemical parameters and yield of winter wheat based on LANDSAT TM images. 2008 IGARSS /2008 IEEE Int Geosci Remote Sens Symp 2: II-789. https://doi.org/10.1109/IGARSS.2008.4779112

Beale CM, Lennon JJ, Gimona A, 2008. Opening the climate envelope reveals no macroscale associations with climate in European birds. Proc Natl Acad Sci 105 (39): 14908-14912. https://doi.org/10.1073/pnas.0803506105

Bolland MDA, 1984. Grain losses due to delayed harvesting of barley and wheat. Aust J Exp Agric 24: 391-395. https://doi.org/10.1071/EA9840391

Bolton DK, Friedl MA, 2013. Forecasting crop yield using remotely sensed vegetation indices and crop phenology metrics. Agric For Meteorol 173: 74-84. https://doi.org/10.1016/j.agrformet.2013.01.007

Boogaard HL, Van Diepen CA, Rotter RP, Cabrera JM, Van Laar HH, 1998. WOFOST 7.1; User's guide for the WOFOST 7.1 crop growth simulation model and WOFOST Control Center 1.5. SC-DLO.

Bougari E, Zaki Dizaji H, Khorasani ME, 2013. Evaluation some affecting factors on John Deere Combine 955series losses during harvest by mathematical models (Case study Ahvaz city). Elixir Agric 58: 15209-15213.

Brisson N, Mary B, Ripoche D, Jeuffroy MH, Ruget F, Nicoullaud B, Gate P, Devienne-Barret F, Antonioletti R, Durr C, Richard G, 1998. STICS: a generic model for the simulation of crops and their water and nitrogen balances. I. Theory and parameterization applied to wheat and corn. Agronomie 18 (5-6): 311-346. https://doi.org/10.1051/agro:19980501

Burnett LC, Bakke AL, 1930. The effect of delayed harvest upon yield of grain. Res Bull Iowa Agric Home Econ Exp Station 10: 1.

Chen C, McNairn H, 2006. A neural network integrated approach for rice crop monitoring. Int J Remote Sens 27: 1367-1393. https://doi.org/10.1080/01431160500421507

De Bernardis C, Vicente-Guijalba F, Martinez-Marin T, Lopez-Sanchez JM, 2016. Particle filter approach for real-time estimation of crop phenological states using time series of NDVI images. Remote Sens 8: 610. https://doi.org/10.3390/rs8070610

Evers JB, Vos J, Yin X, Romero P, Van Der Putten PE, Struik PC, 2010. Simulation of wheat growth and development based on organ-level photosynthesis and assimilate allocation. J Exp Bot 61: 2203-2216. https://doi.org/10.1093/jxb/erq025

Farrer D, Weisz R, Heiniger R, Murphy JP, Pate MH, 2006. Delayed harvest effect on soft red winter wheat in the southeastern USA. Agron J 98: 588-595. https://doi.org/10.2134/agronj2005.0211

Foody GM, 2004. Supervised image classification by MLP and RBF neural networks with and without an exhaustively defined set of classes. Int J Remote Sens 25: 3091-3104. https://doi.org/10.1080/01431160310001648019

Fortin JG, Anctil F, Parent LÉ, Bolinder MA, 2010. A neural network experiment on the site-specific simulation of potato tuber growth in Eastern Canada. Comput Electron Agric 73: 126-132. https://doi.org/10.1016/j.compag.2010.05.011

Galford GL, Mustard JF, Melillo J, Gendrin A, Cerri CC, Cerri CE, 2008. Wavelet analysis of MODIS time series to detect expansion and intensification of row-crop agriculture in Brazil. Remote Sens Environ 112: 576-587. https://doi.org/10.1016/j.rse.2007.05.017

Gao BC, 1996. NDWI□A normalized difference water index for remote sensing of vegetation liquid water from space. Remote Sens Environ 58: 257-266. https://doi.org/10.1016/S0034-4257(96)00067-3

Garroutte EL, Hansen AJ, Lawrence RL, 2016. Using NDVI and EVI to map spatiotemporal variation in the biomass and quality of forage for migratory elk in the Greater Yellowstone Ecosystem. Remote Sens 8: 404. https://doi.org/10.3390/rs8050404

Gitelson AA, Merzlyak MN, 1998. Remote sensing of chlorophyll concentration in higher plant leaves. Adv Sp Res 22: 689-692. https://doi.org/10.1016/S0273-1177(97)01133-2

Gitelson AA, Gritz Y, Merzlyak MN, 2003. Relationships between leaf chlorophyll content and spectral reflectance and algorithms for non-destructive chlorophyll assessment in higher plant leaves. J Plant Physiol 160: 271-282. https://doi.org/10.1078/0176-1617-00887

Govaerts YM, Verstraete MM, Pinty B, Gobron N, 1999. Designing optimal spectral indices: A feasibility and proof of concept study. Int J Remote Sens 20: 1853-1873. https://doi.org/10.1080/014311699212524

Haboudane D, Miller JR, Pattey E, Zarco-Tejada PJ, Strachan IB, 2004. Hyperspectral vegetation indices and novel algorithms for predicting green LAI of crop canopies:

Modeling and validation in the context of precision agriculture. Remote Sens Environ 90: 337-352. https://doi.org/10.1016/j.rse.2003.12.013

Huete AR, 1988. A soil-adjusted vegetation index (SAVI). Remote Sens Environ 25: 295-309. https://doi.org/10.1016/0034-4257(88)90106-X

Huete AR, Liu HQ, Batchily KV, Van Leeuwen WJ, 1997. A comparison of vegetation indices over a global set of TM images for EOS-MODIS. Remote Sens Environ 59: 440-451. https://doi.org/10.1016/S0034-4257(96)00112-5

Jiang Z, Huete AR, Didan K, Miura T, 2008. Development of a two-band enhanced vegetation index without a blue band. Remote Sens Environ 112: 3833-3845. https://doi.org/10.1016/j.rse.2008.06.006

Jin X, Kumar L, Li Z, Xu X, Yang G, Wang J, 2016. Estimation of winter wheat biomass and yield by combining the Aquacrop model and field hyperspectral data. Remote Sens 8: 972. https://doi.org/10.3390/rs8120972

Karimi Y, Prasher SO, Patel RM, Kim SH, 2006. Application of support vector machine technology for weed and nitrogen stress detection in corn. Comput Electron Agric 51: 99-109. https://doi.org/10.1016/j.compag.2005.12.001

Li A, Liang S, Wang A, Qin J, 2007. Estimating crop yield from multi-temporal satellite data using multivariate regression and neural network techniques. Photogramm Eng Remote Sens 73: 1149-1157. https://doi.org/10.14358/PERS.73.10.1149

Li B, Ti C, Zhao Y, Yan X, 2016. Estimating soil moisture with landsat data and its application in extracting the spatial distribution of winter flooded paddies. Remote Sens 8: 38. https://doi.org/10.3390/rs8010038

Liu L, Wang J, Bao Y, Huang W, Ma Z, Zhao C, 2006. Predicting winter wheat condition, grain yield and protein content using multi-temporal EnviSat-ASAR and Landsat TM satellite images. Int J Remote Sens 27 (4): 737-753. https://doi.org/10.1080/01431160500296867

Mansouri-Rad D, 2000. Farm machinery and tractors, Bu-Ali Sina University Press.

McMaster GS, Wilhelm WW, 2003. Phenological responses of wheat and barley to water and temperature: improving simulation models. J Agric Sci 141: 129-147. https://doi.org/10.1017/S0021859603003460

Meng J, Xu J, You X, 2015. Optimizing soybean harvest date using HJ-1 satellite imagery. Precis Agric 16: 164-179. https://doi.org/10.1007/s11119-014-9368-3

Moran D, Pearce D, 1997. Opportunities and limitations for image-based remote sensing in precision crop management. Remote Sens Environ 61: 319-346. https://doi.org/10.1016/S0034-4257(97)00045-X

Moulin S, 1999. Impacts of model parameter uncertainties on crop reflectance estimates: a regional case study on wheat. Int J Remote Sens 20: 213-218. https://doi.org/10.1080/014311699213730

Omer G, Mutanga O, Abdel-Rahman EM, Adam E, 2016. Empirical prediction of leaf area index (LAI) of endangered tree species in intact and fragmented indigenous forests ecosystems using WorldView-2 data and two robust machine learning algorithms. Remote Sens 8: 324. https://doi.org/10.3390/rs8040324

Omid M, Baharlooei A, Ahmadi H, 2009. Modeling drying kinetics of pistachio nuts with multilayer feed-forward neural network. Dry Technol 27: 1069-1077. https://doi.org/10.1080/07373930903218602

Panda SS, Ames DP, Panigrahi S, 2010. Application of vegetation indices for agricultural crop yield prediction using neural network techniques. Remote Sens 2: 673-696. https://doi.org/10.3390/rs2030673

Pantazi XE, Moshou D, Alexandridis T, Whetton RL, Mouazen AM, 2016. Wheat yield prediction using machine learning and advanced sensing techniques. Comput Electron Agric 121: 57-65. https://doi.org/10.1016/j.compag.2015.11.018

Philips PR, O'Callaghan JR, 1974. Cereal harvesting□A mathematical model. J Agric Eng Res 19: 415-433. https://doi.org/10.1016/0021-8634(74)90080-8

Pimentel D, Pimentel MH, 2007. Food, energy, and society. CRC press. https://doi.org/10.1201/9781420046687

Pinter Jr PJ, Hatfield JL, Schepers JS, Barnes EM, Moran MS, Daughtry CS, Upchurch DR, 2003. Remote sensing for crop management. Photogramm Eng Remote Sens 69: 647-664. https://doi.org/10.14358/PERS.69.6.647

Porter JR, Gawith M, 1999. Temperatures and the growth and development of wheat: A review. Eur J Agron 10: 23-36. https://doi.org/10.1016/S1161-0301(98)00047-1

Prasad R, Pandey A, Singh KP, Singh VP, Mishra RK, Singh D, 2012. Retrieval of spinach crop parameters by microwave remote sensing with back propagation artificial neural networks: A comparison of different transfer functions. Adv Sp Res 50: 363-370. https://doi.org/10.1016/j.asr.2012.04.010

Ren J, Chen Z, Zhou Q, Tang H, 2008. Regional yield estimation for winter wheat with MODIS-NDVI data in Shandong, China. Int J Appl Earth Observ Geoinform 10 (4): 403-413. https://doi.org/10.1016/j.jag.2007.11.003

Rocha AV, Shaver GR, 2009. Advantages of a two band EVI calculated from solar and photosynthetically active radiation fluxes. Agr Forest Meteorol 149: 1560-1563. https://doi.org/10.1016/j.agrformet.2009.03.016

Rouse JW, Haas RH, Schell JA, Deering DW, 1974. Monitoring vegetation systems in the Great Plains with ERTS. 3rd ERTS Symp, NASA SP-351, Washington DC. pp: 309-317.

Roy DP, Wulder MA, Loveland TR, Woodcock CE, Allen RG, Anderson MC, Helder D, Irons JR, Johnson DM, Kennedy R, Scambos TA, 2014. Landsat-8: Science and product vision for terrestrial global change research. Remote Sens Environ 145: 154-172. https://doi.org/10.1016/j.rse.2014.02.001

Sabir MS, Igbal M, Yasin M, 2005. Influence of selected combine and crop parameters on kernel damage and threshability of wheat. Pak J Agri Sci 212: 112-116.

Sakamoto T, Wardlow BD, Gitelson AA, Verma SB, Suyker AE, Arkebauer TJ, 2010. A two-step filtering approach for detecting maize and soybean phenology with time-series MODIS data. Remote Sens Environ 114: 2146-2159. https://doi.org/10.1016/j.rse.2010.04.019

Shang J, Liu J, Huffman T, Qian B, Pattey E, Wang J, Zhao T, Geng X, Kroetsch D, Dong T, Lantz N, 2014. Estimating plant area index for monitoring crop growth dynamics using Landsat-8 and RapidEye images. J Appl Remote Sens 8 (1): 085196. https://doi.org/10.1117/1.JRS.8.085196

Streck NA, Weiss A, Xue Q, Baenziger PS, 2003. Improving predictions of developmental stages in winter wheat: A modified Wang and Engel model. Agric For Meteorol 115: 139-150. https://doi.org/10.1016/S0168-1923(02)00228-9

Sun H, Zhang X, Chen S, Pei D, Liu C, 2007. Effects of harvest and sowing time on the performance of the rotation of winter wheat-summer maize in the North China Plain. Ind Crops Prod 25: 239-247. https://doi.org/10.1016/j.indcrop.2006.12.003

Suwannachatkul S, Kasetkasem T, Chumkesornkulkit K, Rakwatin P, Chanwimaluang T, Kumazawa I, 2014. Rice cultivation and harvest date identification based on a hidden Markov model. In: Electrical Engineering/Electronics, Computer, Telecommunications and Information Technology (ECTI-CON), 11th Int Conf on IEEE, pp: 1-6. https://doi.org/10.1109/ECTICon.2014.6839856

Therond O, Hengsdijk H, Casellas E, Wallach D, Adam M, Belhouchette H, Oomen R, Russell G, Ewert F, Bergez JE, Janssen S, 2011. Using a cropping system model at regional scale: Low-data approaches for crop management information and model calibration. Agric Ecosyst Environ 142: 85-94. https://doi.org/10.1016/j.agee.2010.05.007

Vincini M, Frazzi E, D'alessio P, Stafford JV, 2007. Comparison of narrow-band and broad-band vegetation indexes for canopy chlorophyll density estimation in sugar beet. In: Proc 6th Eur Conf on Precis Agric, pp: 189-196.

Viña A, Gitelson AA, Nguy-Robertson AL, Peng Y, 2011. Comparison of different vegetation indices for the remote assessment of green leaf area index of crops. Remote Sens Environ 115: 3468-3478. https://doi.org/10.1016/j.rse.2011.08.010

Wang J, Huang JF, Wang XZ, Jin MT, Zhou Z, Guo QY, Zhao ZW, Huang WJ, Zhang Y, Song XD, 2015. Estimation of rice phenology date using integrated HJ-1 CCD and Landsat-8 OLI vegetation indices time-series images. J Zhejiang Univ Sci B 16 (10): 832-844. https://doi.org/10.1631/jzus.B1500087

Xie Y, Sha Z, Yu M, Bai Y, Zhang L, 2009. A comparison of two models with Landsat data for estimating above ground grassland biomass in Inner Mongolia, China. Ecol Modell 220: 1810-1818. https://doi.org/10.1016/j.ecolmodel.2009.04.025